KU LEUVEN

FACULTEIT
INGENIEURSWETENSCHAPPEN

B-KUL-H04X3A: Control Theory

Team members:

Lefebure Tiebert (r0887630)
Campaert Lukas (r0885501)

Assignment 2: Velocity Control of the Cart

Professor:

Prof. Dr. Ir. Jan Swevers

Academic Year 2025-2026

Declaration of Originality

We hereby declare that this submitted draft is entirely our own, subject to feedback and support given us by the didactic team, and subject to lawful cooperation which was agreed with the same didactic team. Regarding this draft, we also declare that:

1. *Note has been taken of the text on academic integrity* `https://eng.kuleuven.be/studeren/masterproef-en-papers/documenten/20161221-academischeintegriteit-okt2016.pdf`.
2. *No plagiarism has been committed as described on* `https://eng.kuleuven.be/studeren/masterproef-en-papers/plagiaat#Definitie:%20wat%20is%20plagiaat?`.
3. *All experiments, tests, measurements, …, have been performed as described in this draft, and no data or measurement results have been manipulated.*
4. *All sources employed in this draft - including internet sources - have been correctly referenced.*

1 Design of a velocity controller using the frequency response method

1.1 Controller type choice

To achieve zero steady-state error on a constant velocity reference, which requires a closed-loop system with type 1 behavior, the controller must provide infinite DC gain. The identified DC-motor dynamics contain no inherent integrator, meaning proportional (P), PD, or lead-type controllers would leave a nonzero steady-state error. Desired closed-loop properties include:

- Zero steady-state error on constant velocity
- Adequate robustness (sufficient phase margin)
- Sufficient bandwidth for accurate velocity tracking
- Low sensitivity to external disturbances (slope, friction)

Possible controller structures:

- P / PD: no integrator, meaning a nonzero steady-state error
- Lead: increases phase margin but does not provide infinite DC gain
- Lag: increases low-frequency gain but insufficient for zero error
- PI: provides an integrator and a zero for phase correction

The PI compensator is selected as a suitable controller. The continuous-time PI compensator is:

$$D(s) = \frac{K}{s}(s + \frac{1}{T_i}) \tag{1}$$

where:

- K = proportional gain
- T_i = integration time

The controller increases system type by 1 and ensures infinite DC gain:

$$\lim_{s \to 0} D(s) = \infty \tag{2}$$

which ensures zero steady-state error for step velocity references and offers straightforward tuning in the frequency domain, making it highly suitable for motor velocity control.

1.2 Design process and design parameters choices

The controller parameters were obtained using the frequency-response method, based on the identified motor model $G_s(s)$ from Assignment 1, both for motor A and motor B. The simplified continuous-time models after filtering are:

$$G_{s,A}(s) = \frac{0.3677s^2 - 147.1s + 1.471e04}{s^2 + 237.1s + 7413} \tag{3}$$

$$G_{s,B}(s) = \frac{0.3763s^2 - 150.5s + 1.505e04}{s^2 + 237s + 7408} \tag{4}$$

Choice of cross-over frequency ω_c: The cross-over frequency determines the closed-loop bandwidth. A value must balance:

- Faster response vs. actuator limitations
- Tracking performance vs. noise sensitivity
- Stability margin vs. speed

A phase margin (PM) target of 55° was imposed to ensure robust behavior. The uncompensated phase of the motor model was evaluated to find the frequency satisfying:

$$\phi_G(\omega_c) = -180^\circ + PM + \phi_{PI}(\omega_c) \tag{5}$$

where:

- $\phi_G(\omega_c)$ is the phase of the uncompensated open-loop system at ω_c
- PM is the desired phase margin, which is 55°
- $\phi_{PI}(\omega_c)$ is the anticipated phase lag of the PI compensator at ω_c, which is selected to be 15°

This yields:

$$\phi_G(\omega_c) = -180^\circ + 55^\circ + 15^\circ = -110^\circ \tag{6}$$

The cross-over frequency ω_c where the phase of the uncompensated open-loop system equals -110° is fixed directly by the specification:

$$\omega_{c,A} = \omega_{c,B} = 60 \text{ rad/s}, \qquad \omega_{c,\text{low}} = 2\pi \cdot 0.5 \text{ rad/s} \tag{7}$$

Integration time $\mathbf{T}_i$: The integrator pole must lie well below the cross-over frequency to avoid excessive phase lag. The integration time is selected such that the contribution of the PI compensator to the phase at ω_c equals the anticipated one ($\phi_{PI}(\omega_c) = 15^\circ$). This design rule is mathematically expressed as:

$$T_i\omega_c = \tan(90^\circ - \phi_{PI}(\omega_c)) \tag{8}$$

using a margin of $\phi_{PI}(\omega_c) = 15^\circ$, leading to:

$$T_{i,A} = T_{i,B} \approx 0.062 \text{ s}, \qquad T_{i,\text{low}} \approx 1.19 \text{ s} \tag{9}$$

Interpretation of trade-offs:

- A smaller T_i gives faster removal of steady-state error but adds more phase lag.
- A larger T_i reduces phase lag but slows integral action.

Proportional gain K: The gain is calculated such that the gain of the compensated system at ω_c equals 1:

$$|D(j\omega_c)G(j\omega_c)| = 1 \tag{10}$$

The continuous controller is discretized using the Tustin method (with $c2d$ MATLAB command), and the gain is adjusted iteratively until MATLAB's Bode diagram confirms the desired cross-over frequency. The identified wheel models yield proportional gains obtained from the unity-gain condition $|D(j\omega_c)G(j\omega_c)| = 1$; the MATLAB script prints these numerical values (for nominal and low-bandwidth controllers) and the same numbers are exported to the Arduino coefficients.

Design trade-offs:

- Increasing PM provides robustness and damping but slows the response.
- Increasing K increases bandwith but reduces phase margin (PM), raising the risk of oscillatory behavior and actuator saturation.
- Increasing T_i reduces phase lag but slows convergence to steady-state (decreased integral speed).
- Increasing ω_c reduces delay sensitivity but amplifies encoder noise.

Verification requirements: The open-loop Bode plot $L(j\omega) = D(j\omega)G(j\omega)$ must show:

- Unity gain ($|L(j\omega)| = 0dB$) at ω_c
- $PM \approx 55°$
- PI zero (at $\omega_z = \frac{1}{T_i}$) far below ω_c

The time-domain verification must confirm:

- Zero steady-state error on constant velocity reference
- Acceptable rise time ($t_r < 0.5$s) and overshoot ($M_p < 20\%$)

Bode Diagram Verification: Figures 1 and 2 show the compensated open- and closed-loop responses for both motors. The open-loop plots highlight the unity-gain crossover at $\omega_c = 60$ rad/s with a phase margin of roughly 55°, and the closed-loop plots show that the resulting bandwidth is about the chosen crossover with a modest resonant peak.

1.3 Theoretical and practical closed-loop bandwidth limitations

Theoretical limitation: The bandwidth cannot exceed the frequency where the total open-loop phase ϕ_L approaches $-180°$. Beyond this point, increasing the gain drives the closed-loop system toward instability. For a first-order motor model, this typically limits cross-over frequency to approximately:

$$\omega_c \approx \frac{1}{\tau} \tag{11}$$

where τ is the motor time constant.

Practical limitations:

- Sampling frequency (100 Hz): Nyquist limit of 50 Hz ($= f_s/2$) cuts off the maximum achievable bandwidth.
- Microcontroller delay introduces extra phase lag, reducing stability margins.
- Voltage saturation (≈ 12 V) limits achievable proportional gain.
- Encoder quantization noise leads to large high-frequency disturbances when bandwidth is too high.
- Motor friction and unmodeled nonlinearities reduce agreement with the designed frequency response.

These constraints limit the achievable closed-loop bandwidth even if theoretically higher values are possible.

2 Experimental validation of the designed controller

2.1 Step response validation

Experiment: A constant velocity reference of 10 rad/s is applied to both motors. The measured velocity is compared to the simulated velocity (using the compensated model).

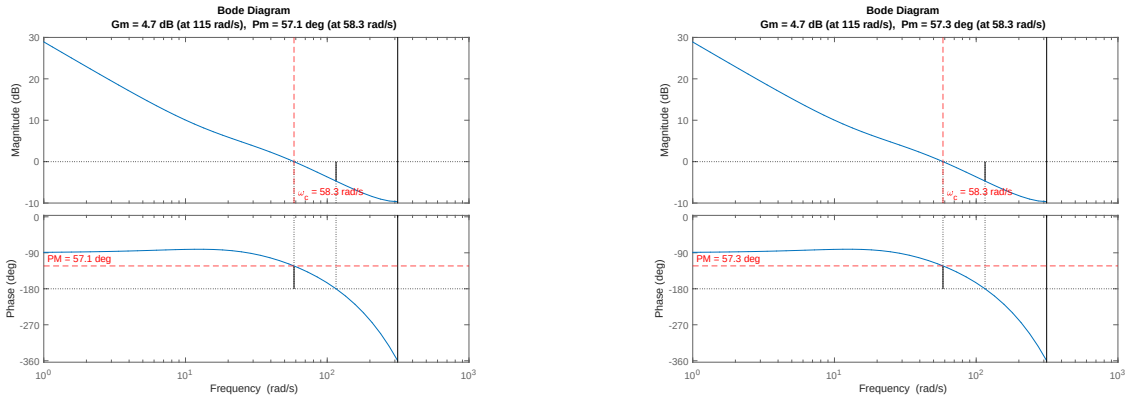

(a) Motor A

(b) Motor B

Figure 1: Open-loop Bode diagram showing cross-over frequency ω_c and phase margin.

Step response: The measured and simulated closed-loop responses exhibit similar transient patterns. Initial delays and rise times closely match the model predictions, confirming the validity of the identified motor dynamics. The steady-state velocity converges to the reference value of 10 rad/s, demonstrating correct integral action. Oscillations in the measured signal may be slightly larger than in the simulation due to encoder quantization, unmodeled friction, and voltage saturation clipping. Despite these differences, the measured response remains consistent with expected closed-loop behavior.

Figure 3 compares the measured and simulated step responses for both motors; each plot shows the step reference (dotted), measured response (solid), and simulation (dashed).

Tracking error: The initial tracking error matches the simulated transient and decays to approximately zero, apart from small steady-state fluctuations caused by sensor noise.

Figure 4 shows the tracking error comparison for both motors (measured: solid; simulated: dashed).

Control signal (voltage): The control voltage initially spikes due to a large tracking error. The measured signal is clipped at roughly 12 V due to hardware limits. This clipping creates a slightly lower first overshoot compared to the simulation. The control signal tracks the evolution of the velocity error as expected.

Figure 5 reports the measured and simulated control voltages (measured: solid; simulated: dashed).

Performance characteristics: Rise time (t_r), overshoot (M_p) and settling time (t_s) align with the design specifications. The measured and simulated responses show closely matching dynamic properties. The rise time t_r of the measured system is slightly slower than in simulation due to unmodeled friction and voltage saturation, whereas the steady-state value is identical, confirming correct integral action. The overshoot M_p matches well in shape but is marginally larger in the experiment because encoder quantization and actuator

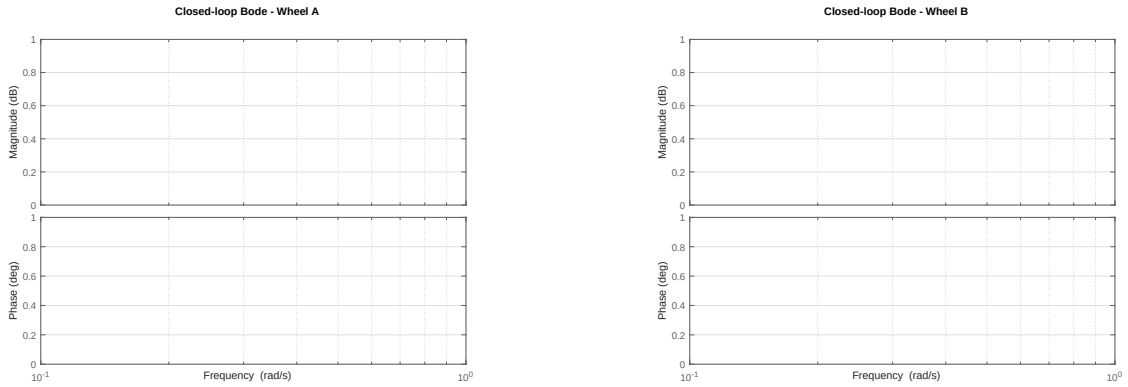

(a) Motor A (b) Motor B

Figure 2: Closed-loop Bode magnitude showing bandwidth ω_{BW}.

limits introduce additional damping and asymmetry. The settling time t_s remains consistent between measurement and simulation, indicating that the designed phase margin ($PM = 55°$) and bandwidth translate reliably to the real hardware. Overall, the measured performance agrees with the designed characteristics: fast but well-damped convergence, full elimination of steady-state error, and control behavior that remains within actuator limits.

2.2 Steady-state performance under constant force disturbance

Experiment: The cart is placed on an incline so that gravity (constant acceleration $g = 9.81\ m/s^2$) produces a constant negative torque, opposing the motion, on both wheels. The same velocity setpoint as in Section 2.1 is applied, namely a constant velocity reference of 10 rad/s.

Block diagram: The constant force disturbance signal enters the loop as an external load torque acting on the motor dynamics. The disturbance affects the transient velocity, but the PI controller gradually compensates through its integral action.

Step response with disturbance: The measured response shows lower peaks and a slower rise than the nominal case, while the simulated response remains unchanged because it does not include the disturbance. Despite this mismatch in the transient, both measured and simulated curves converge to the same steady-state value due to the integrator, which compensates the constant load.

Figure 6 shows the disturbed step response for both motors (reference: dotted; measured: solid; simulated: dashed).

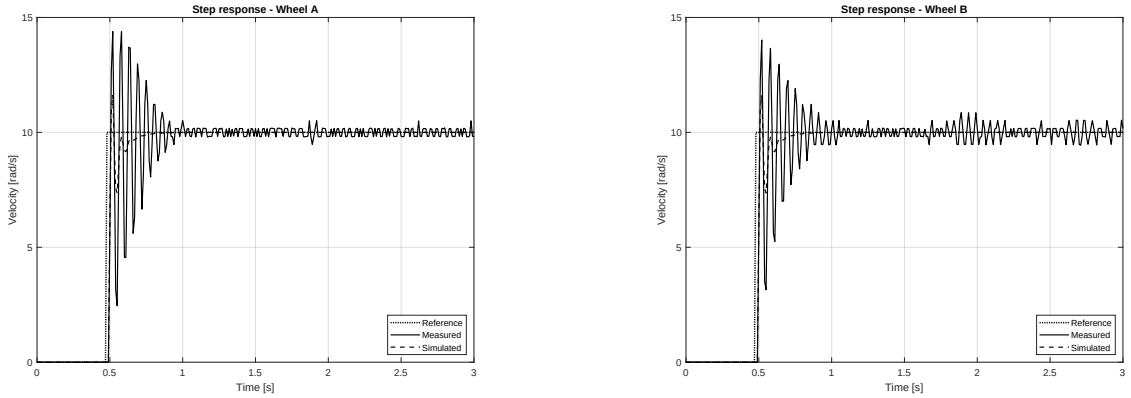

(a) Motor A

(b) Motor B

Figure 3: Step response on flat ground: reference (dotted) vs. measured (solid) vs. simulated (dashed).

Tracking error with disturbance: The measured tracking error is larger at the start and decays more smoothly, whereas the simulated error follows the original undisturbed transient. Both measured and simulated tracking error eventually settle close to zero, but only the measured curve reflects the effect of the disturbance.

Figure 7 reports the tracking error under the constant disturbance (measured: solid; simulated: dashed).

Control signal with disturbance: The measured control signal settles at a visibly higher steady-state value than the simulated one, which remains unchanged without the disturbance term. The transient shapes remain similar, but only the measured control effort compensates for the additional load.

Figure 8 shows the control signal comparison with disturbance for both motors. The measured (solid line) and simulated (dashed line) control signal of the step reference are shown in one plot.

Figure 8 shows the associated control voltage comparison (measured: solid; simulated: dashed).

Reference tracking despite disturbance: The controller continues to track the reference in steady state because the integral action of the PI controller compensates any constant disturbance by increasing the steady-state control effort until the velocity error becomes zero again. Although the transient response is slowed down by the opposing force/torque, the integrator removes the steady-state error for constant disturbances, so the reference is still tracked.

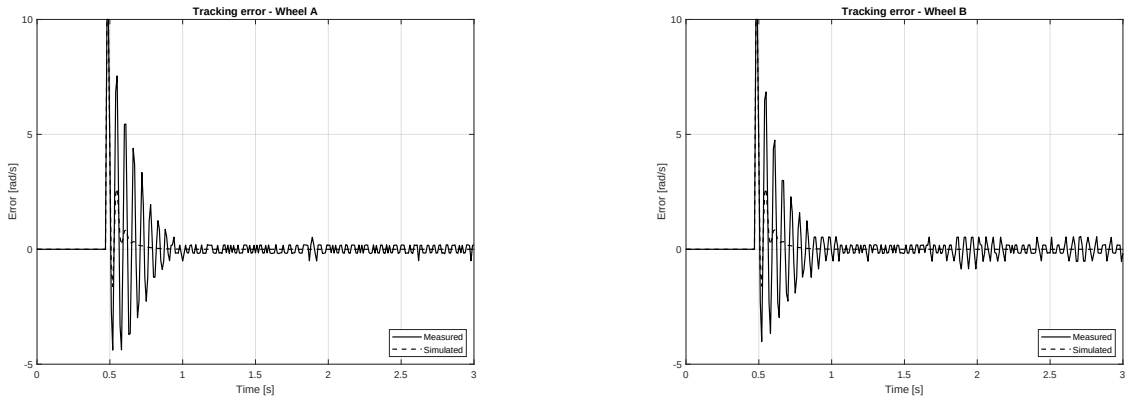

(a) Motor A

(b) Motor B

Figure 4: Tracking error on flat ground: measured (solid) vs. simulated (dashed).

3 Controller validation with a cross-over frequency ω_c of 0.5 Hz (including constant disturbance)

Experiment: With the redesigned PI controller, the cross-over frequency is reduced to about 0.5 Hz, which lowers the closed-loop bandwidth and yields a more conservative controller. The same constant disturbance (cart on a ramp) is applied and the plots of step response, tracking error and control signal now contain both controllers (high-bandwidth from Section 2.2 and low-bandwidth from Section 2.3).

Step response with low-bandwidth (and disturbance): The measured response with the low-bandwidth controller rises visibly slower and shows almost no overshoot, whereas the high-bandwidth controller from Section 2.2 reacts faster and exhibits more pronounced transient peaks. The simulated curves follow the same trend for each controller, but differences between measured and simulated responses remain slightly larger for the high-bandwidth case because it is more sensitive to model errors and disturbance effects.

Figure 9 shows the step response comparison for both motors. The step reference (dotted line), measured closed-loop response (solid line) and simulated closed-loop response (dashed line) are shown in one plot, both for the high-bandwidth and low-bandwidth case.

Tracking error with low-bandwidth (and disturbance): For the low-bandwidth controller the tracking error decreases more gradually with a smooth, almost aperiodic decay and small oscillations, while the high-bandwidth controller produces a quicker error reduction but with larger overshoot and ringing. In both cases the steady-state tracking error remains close to zero, confirming that the integral action compensates the constant disturbance. The low-bandwidth controller, however, needs more time to eliminate the error.

Figure 10 shows the tracking error comparison for both motors. The measured (solid line) and simulated (dashed line) tracking error of the step reference are shown in one plot, both for the high-bandwidth and

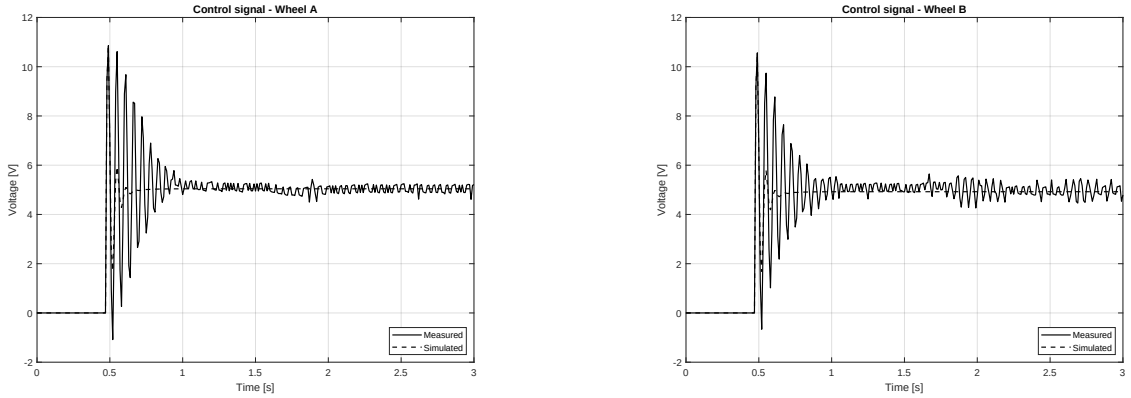

(a) Motor A

(b) Motor B

Figure 5: Control voltage on flat ground: measured (solid) vs. simulated (dashed). Saturation at ≈ 12 V is visible.

low-bandwidth case.

Control signal with low-bandwidth (and disturbance): The measured control signal of the low-bandwidth controller has clearly smaller peaks and a smoother shape, but its steady-state voltage is comparable to or slightly higher than in Section 2.2, since the same disturbance torque must be balanced. The high-bandwidth controller generates sharper transients and larger initial control peaks, which push the actuator closer to saturation and amplify noise. The simulated control signals show the same qualitative difference between both designs.

Figure 11 shows the control signal comparison for both motors. The measured (solid line) and simulated (dashed line) control signal of the step reference are shown in one plot, both for the high-bandwidth and low-bandwidth case.

Contribution of the different (PI) controller parts: For the high-bandwidth controller, the proportional term (P) dominates the fast reaction to changes, resulting in rapid initial acceleration and stronger overshoot, while the integrator (I) mainly removes the residual steady-state error under disturbance. In the low-bandwidth design, the proportional gain K is reduced and the cross-over frequency ω_c is lower, so the proportional action (P) reacts more slowly and the integrator (I) builds up more gradually. This combination yields smoother, more damped responses with reduced peak control effort, at the cost of a slower convergence to the reference.

References

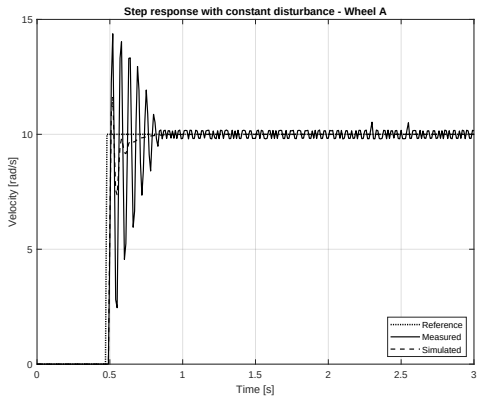

(a) Motor A

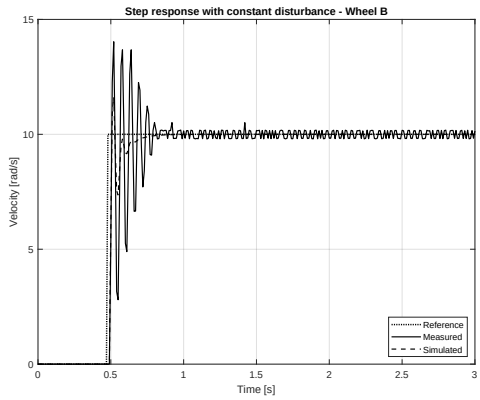

(b) Motor B

Figure 6: Step response on the incline: reference (dotted) vs. measured (solid) vs. simulated (dashed).

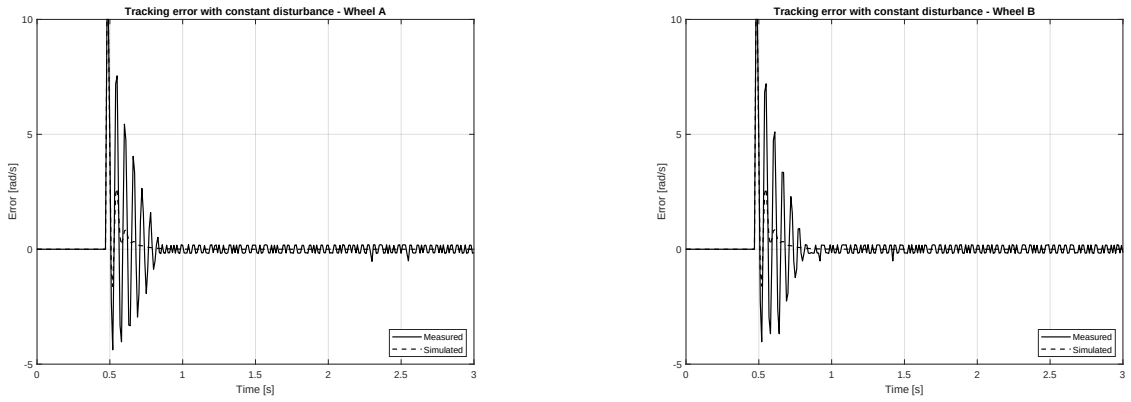

(a) Motor A

(b) Motor B

Figure 7: Tracking error with constant disturbance: measured (solid) vs. simulated (dashed).

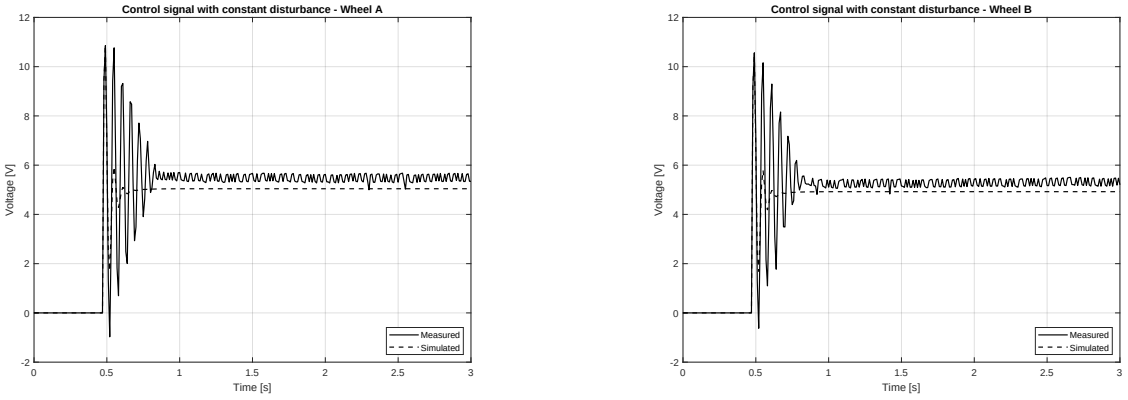

(a) Motor A

(b) Motor B

Figure 8: Control voltage with constant disturbance: measured (solid) vs. simulated (dashed).

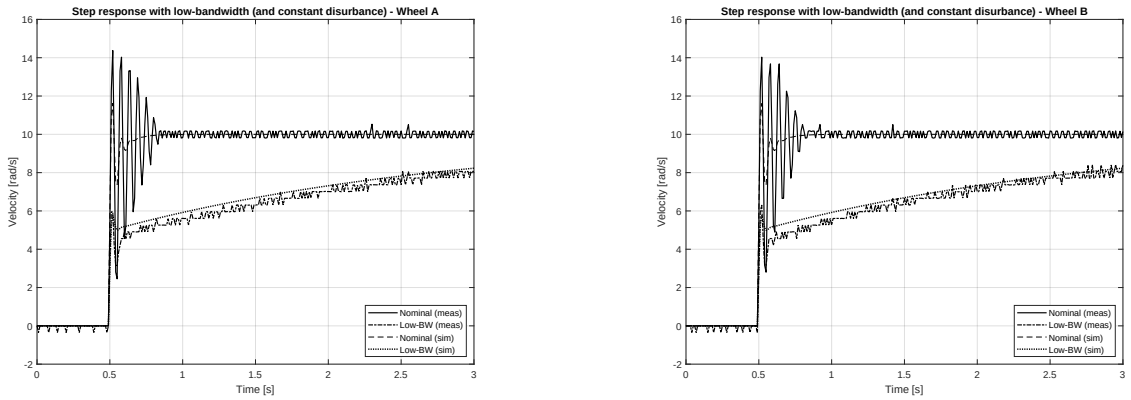

(a) Motor A

(b) Motor B

Figure 9: Step response comparison: nominal controller vs. low-bandwidth controller on the incline.

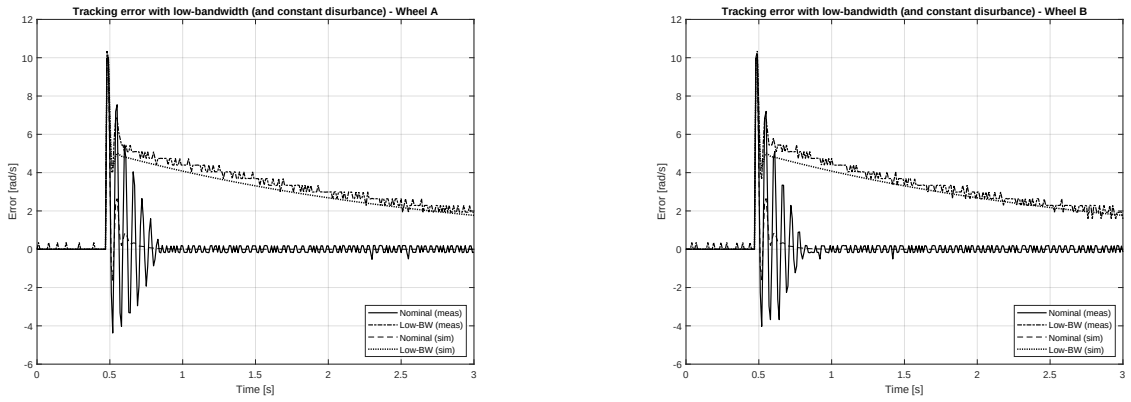

(a) Motor A

(b) Motor B

Figure 10: Tracking error comparison: nominal controller vs. low-bandwidth controller on the incline.

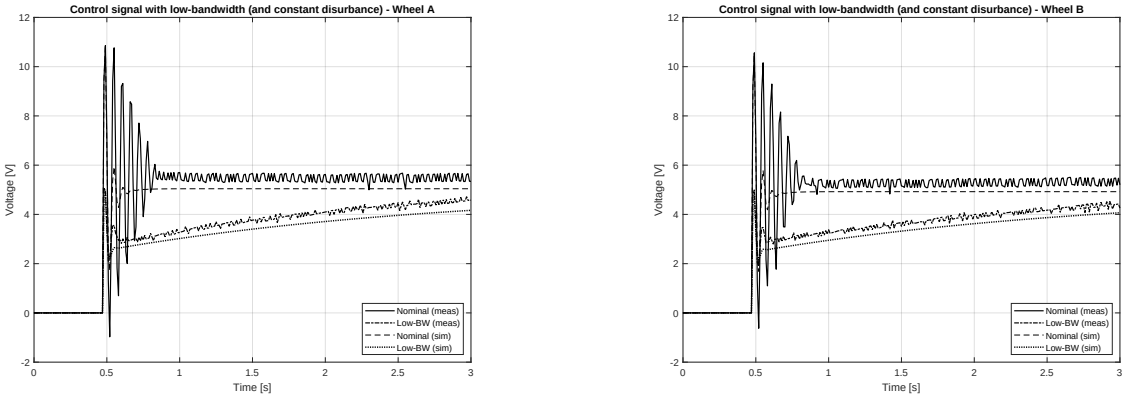

(a) Motor A

(b) Motor B

Figure 11: Control voltage comparison: nominal controller vs. low-bandwidth controller on the incline.